# Achromatic Trajectories and Lunar Material Transport for Space Colonization

T. A. Heppenheimer*
*Center for Space Science, Fountain Valley, Calif.*

**An overview is presented of the main features of the dynamical problems associated with the large-scale launching of lunar mass, as required for space colonization. The mass-transport mode treated involves ballistic flight from the lunar surface to a mass-catcher near the L2 libration point. A theoretical treatment is given for a new effect of trajectories in rotating coordinate systems: that their arrival accuracy or sensitivity may be proportional, not (as is usual) to launch velocity error, but rather to the square of this error. Such trajectories are called "achromatic." A method is presented to find them. This method is used in the circular restricted three-body problem to generate maps of key parameters associated with mass-catching near L2. A renormalization of initial conditions in the elliptic restricted three-body problem permits the construction of similar maps for the case of lunar eccentricity (0.0549) as well. Applications of these results include selection of an optimal mass-driver lunar site and orientation, and derivation of the catcher equations. The latter are linearized equations with nonperiodic time-varying coefficients describing the motion of the catcher under all constraints associated with its operation.**

## Introduction

THE colonization of space will rely upon the large-scale transport and use of material resources available in space. The use of lunar resources is especially attractive, and the problem of lunar mass transport has received attention. Earlier contributions[1,2] outlined the major features of the methods which currently appear most promising. In particular, Ref. 1 gave the theoretical background for certain of the developments to be presented here.

The selected mass-transport method involves launch by mass-driver (electromagnetic accelerator) of packages of lunar material, which follow ballistic trajectories to a mass-catcher near L2. Reference 1 treated these trajectories and showed the existence of a launch site for which the sensitivity or arrival accuracy, if regarded as proportional to the launch velocity error, is zero.

The proportionality of arrival error to velocity error is embodied in such familiar concepts as "error ellipse" and "circular error probable." The vanishing of this linear proportionality, for the trajectories treated here, represents a newly identified effect of trajectories in rotating coordinate systems. This paper elaborates the nature of this effect via new theorems, which lead to practical methods for the engineering application of this new effect. The theme of this paper then is the development of the insights required for such engineering applications. Of particular concern is the derivation of equations for mass-catcher motion. Further work gives optimal catcher trajectories based on these equations,[3] and treats the problem of transfer of lunar material from the catcher to an optimal space-colony location.[4]

## Achromatic Trajectories

It is possible to launch payloads on ballistic trajectories from the lunar surface to a selected point in space such that the miss distance at the target is proportional to the square of the error in a selected component of launch velocity. The associated launch site is described as a critical point, and the resultant trajectories are described as achromatic. The existence of achromatic trajectories was first demonstrated by numerical computation on July 19, 1976. The terminology "achromatic" derives from the action of achromatic lenses in focusing light of diverse wavelengths to a common focus, this action being due to the vanishing of a wavelength-dependent derivative (dispersion coefficient). The "focusing" action of achromatic trajectories results from the vanishing of a velocity-dependent derivative (sensitivity coefficient). In Ref. 1, it is shown that sensitivities due to errors in along-track velocity ($V_T$) are ~1000-5000 m/mm/s of launch velocity error, which is up to two orders or magnitude larger than those due to errors in velocity normal to the lunar surface ($V_N$) and up to three orders larger than those due to cross-track ($V_Z$) errors, when the mass-driver track lies in the lunar equator. So, in this paper, only $V_T$-insensitive achromatic trajectories are treated.

In Ref. 1, the existence and character of achromatic trajectories was considered using aspects of the topological properties of continuous mappings. However, much insight can be gained into their nature through consideration of two-body motion (Fig. 1).

Consider a family of trajectories resulting from tangential launches from the surface of a sphere. Let there be a test body in orbit, moving with angular velocity $df/dt=n$. Now consider a trajectory resulting from launch with velocity $V_{T0}$, passing a distance $r=r_0$ from the planet center with flight time $t_{f0}$ and reaching $r=r_0$ at true anomaly $f=f_0$. Let the launch velocity suffer a perturbation, $V_T=V_{T0}+\epsilon$. Suppose the perturbed trajectory passes $r=r_0$ with flight time $t_{f0}-\Delta t_f$ and at true anomaly $f=f_0-n\Delta t_f$. Then, in a coordinate system rotating with the test body, the two trajectories are seen to cross at $r=r_0$. Now, following Ref. 1, define a linear sensitivity coefficient:

$$C_{VT}=\frac{\text{Miss distance}}{\Delta V_T} \quad \text{m/mm/s} \tag{1}$$

In Ref. 1, the following theorem is proved:

*Theorem 1* The condition that $C_{VT}=0$, for launch from longitude $\lambda=\lambda_0$, is that $\lambda_0$ be the branch point joining two families of trajectories passing through $r=r_0$, one with $\partial\lambda/\partial V_T\leq 0$ and the other with $\partial\lambda/\partial C_T\geq 0$.

Received Aug. 8, 1977; revision received Feb. 17, 1978. 

Index category: Lunar and Interplanetary Trajectories.

*Chief Scientist. Member AIAA.

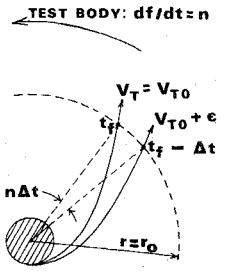


Fig. 1 The physical character of achromaticity.

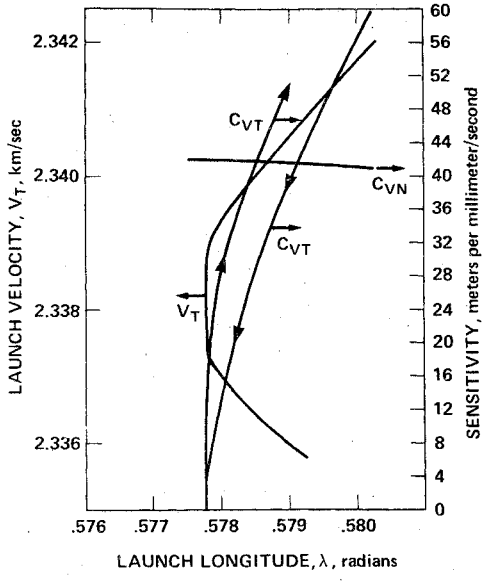


Fig. 2 Application of Theorem 1 from Ref. 1.

Figure 2 illustrates a numerical test of this theorem, for which the trajectories originate from the lunar surface and pass through L2. Here $C_{VT}=0$ for $\lambda_0=0.577768148$; the existence of the branch point is evident.

*Theorem 2* The two-body trajectory of Fig. 1, for which $C_{VT}=0$ at $r=r_0$, is unique.

*Proof* This trajectory is a planar conic, defined uniquely by orbital elements $a, e, \tilde{\omega}, f_0$, where $f_0$ is $f$ at $r=r_0$. These four quantities are determined uniquely by the following four equations:

$$\tilde{\omega}=\lambda_0 \text{ (launch site longitude)} \tag{2a}$$

$$a(1-e)=r_p \text{ (planet radius)} \tag{2b}$$

$$a(1-e^2)/(1+e\cos f_0)=r_0 \tag{2c}$$

$$n\partial t_f/\partial V_T=\partial f_{r=r_0}/\partial V_T \tag{2d}$$

With no loss of generality, choose a target point $P$ to lie at $r=r_0$ on the line joining the test body and planet center. Also choose a longitude reference by specifying $n=$ planet rotation rate.

*Theorem 3* The cited trajectory is such that for $V_T \geq V_{T0}$, $\partial\lambda/\partial V_T \geq 0$ and for $V_T \leq V_{T0}$, $\partial\lambda/\partial V_T \leq 0$.

*Proof* For $V_T=V_{T0}$, Eq. (2d) implies $\partial\lambda/\partial V_T=0$. For $V_T<V_{T0}$, one has $n\partial t_f/\partial V_T > \partial f_{r=r_0}/\partial V_T$, so that for launch from longitude $\lambda=\lambda_0$ the trajectory reaches $r=r_0$ with $t_f > t_{f0}+n\Delta t_f$, which is "too late" to hit $P$. Hence $\lambda$ must be increased and $\partial\lambda/\partial V_T<0$. For $V_T>V_{T0}$, one has $\partial f_{r=r_0}/\partial V_T > n\partial t/\partial V_T$, so that for launch from $\lambda_0$ the trajectory reaches $r=r_0$ with $f<f_0-n\Delta t_f$, and the trajectory is "too flat" to hit $P$. Hence $\lambda$ must be increased and $\partial\lambda/\partial V_T>0$.

The cited nominal trajectory thus is achromatic, according to Theorem 1 and Ref. 1. These results then may be generalized.

*Theorem 4* The existence of achromatic trajectories is an effect associated with rotating coordinate systems and in no way depends on the specific properties of the restricted three-body problem or of any other dynamical model adopted.

*Proof* The association of achromatic trajectories with rotating coordinates follows from Fig. 1. By definition, an achromatic trajectory has $C_{VT}=0$. By Theorems 1 and 3, $C_{VT}=0$ if and only if $n\,\partial t_f/\partial V_T=\partial f_{r=r_0}/\partial V_T$. But this latter condition may be satisfied for trajectories in general and does not require any particular dynamical model; for one may always write $r=r(f;\,t)$ as representing a trajectory launched tangentially from $\lambda_0$ with given $V_T$.

One now requires a method for finding focus points for achromatic trajectories. For a specified launch site, the focus point for an achromatic trajectory with given $V_T$ is found by integrating two neighboring trajectories in an appropriate rotating coordinate system, launched tangentially with respective velocities $V_T$ and $V_T+\epsilon$, $\epsilon\neq 0$, and $\epsilon \ll V_T$. The focus point then is the point where the two trajectories cross, since $C_{VT}=0$ at that point.

In using this method, one considers that trajectories are integrated numerically and are known, not as continuous curves, but as discrete specifications of state vectors printed out no more frequently than once each integration step. Hence, for integrations in the plane, let $(x_1, y_1, \dot{x}_1, \dot{y}_1)$ be the state vector for the trajectory launched with $V_T$, $(x_2, y_2, \dot{x}_2, \dot{y}_2)$ the state vector for that launched with $V_T+\epsilon$. Then near the focus point, there exist time increments $\Delta t_1$, $\Delta t_2$ such that

$$x_1+\dot{x}_1\Delta t_1 = x_2+\dot{x}_2\Delta t_2 \tag{3a}$$

$$y_1+\dot{y}_1\Delta t_1 = y_2+\dot{y}_2\Delta t_2 \tag{3b}$$

Then at each integration step, $\Delta t_1$ is computed and, providing the determinant $(\dot{x}_2\,\dot{y}_1-\dot{x}_1\,\dot{y}_2)\neq 0$, the focus point lies between the two integration steps for which $\Delta t_1$ changes sign. It then is located more precisely by interpolation. The determinant vanishes when the two trajectories are parallel. Thus, by keeping track of this determinant, one distinguishes between parallelism and crossing. It is also possible that $\Delta t_1$ and the determinant vanish simultaneously. Then the two trajectories are locally tangent where they cross.

The geometry of the crossing is given in Fig. 3. Here $\Delta\gamma$ is the angle at crossing and $\Delta x$ is the deviation in the location of the crossing point from the catcher location. The miss distance $\Delta y$,

$$\Delta y=\epsilon^2\,(\partial\Delta\gamma/\partial V_T)\,(\partial\Delta x/\partial V_T) \tag{4}$$

is quadratic in the launch velocity error. The ordinary situation, in which $\Delta y \propto \epsilon$, thus does not apply, and one cannot regard the dispersion in impact points, due to errors in $V_T$ and (for example) $V_Z$, as giving rise to an error ellipse. Instead, the pattern of the impact lies within a curve shaped like the letter "D." An approximately symmetric error ellipse results only if allowed errors in $V_T$ produce much less dispersion than allowed errors in $V_N$.

By extension of Fig. 3, consider a family of crossing trajectories resulting from launch with neighboring values of $V_T$ (Fig. 4). Such a family possesses an envelope, every point of which is tangent to a trajectory and is associated with a given $V_T$. Any point on this envelope thus can be reached via an achromatic trajectory. This envelope, hereafter referred to as a focus locus, is the cynosure of further attention. One is concerned with the study of focus loci rather than of trajectories; the trajectories lose their character as being directly of interest, and instead serve merely as the function or mapping connecting initial values $(\lambda_0, V_T)$ to points $(x, y)$ on the focus loci.

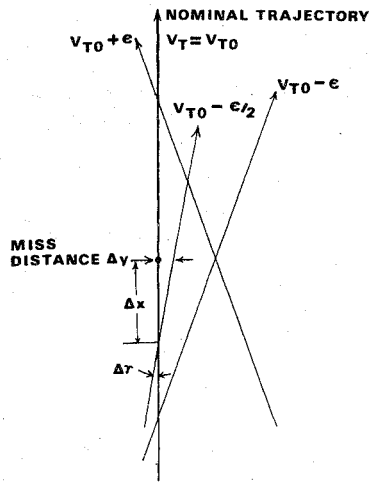


Fig. 3 The geometry of a focus point.

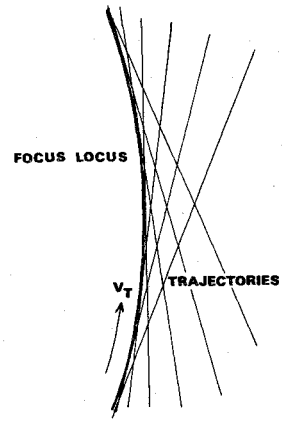


Fig. 4 Definition of a focus locus.

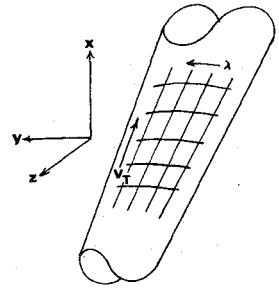


Fig. 5 Representation of focus loci as a mapping on a cylinder.

The preceding discussion applies to trajectories lying in the plane of the planet equator. For three-dimensional trajectories, the analogs of Eqs. (3) do not generally possess solutions. However, Ref. 1 showed that $V_Z$ errors give the least sensitive effects, 5 m/mm/s or less, so for nearly planar trajectories it will be seen that the principal effect of the out-of-plane motion is to limit the errors in $V_T$ which Eq. (4) would otherwise allow. Achromatic trajectories then can result for large ranges of $V_T$ and $\lambda$ and for moderate ranges of launch latitude $\beta$. There then results, for $V_T$, $\lambda$, $\beta$ varying arbitrarily, a continuous volume of points each of which is a focus point for an achromatic trajectory.

In this paper, $\beta$ and $\lambda$ are not considered to so vary. Rather, we consider a fixed mass-driver installation on the Moon, so that $\lambda$ and $\beta$ vary principally in response to the lunar librations in longitude and latitude. Hence, for time periods of ~ 1 month, the set of focus loci associated with the fixed launch site constitutes a cylinder (Fig. 5). One now considers the mapping of parameters on such a cylinder.

## Lunar Mass Transport

### Lunar Motions

Discussions of lunar motions appear in Ref. 5 and elsewhere. The results given here are needed for the present work.

The libration in latitude $\Delta\beta$ results from the lunar obliquity on its orbital plane, which has the constant value 6 deg, 40 min, 44s. $\Delta\beta$ has approximately this value as its amplitude; the period is one draconitic month (time between successive passages of the ascending node on the ecliptic) which is 27.212220 days.

The libration in longitude $\Delta\lambda$ results from lunar eccentricity $e_m$ and is very nearly $\Delta\lambda \sim$ (mean anomaly) − (true anomaly):[6]

$$\Delta\lambda = -2[B(1+\cos\phi)\sin f_m - B^2(\tfrac{1}{2}+\cos\phi)\sin 2f_m + B^3(\tfrac{1}{3}+\cos\phi)\sin 3f_m + \ldots] \quad (5)$$

where

$$\cos\phi = (1-e_m{}^2)^{\frac{1}{2}}$$

$$B = \tan(\phi/2) = (1/e_m)[1-(1-e_m{}^2)^{\frac{1}{2}}]$$

and $f_m$ = true anomaly. The period is one anomalistic month (time between successive perihelion passenges), 27.5545503 days. So $\Delta\lambda$, $\Delta\beta$ are not in phase; their variations trace out a Lissajous curve which, in any month, is geometrically proportional to the cross section of the cylinder of Fig. 5. Further, $e_m$ varies from 0.0432 to 0.0666 with mean of 0.0549. The principal contribution to this effect has period 206.26735 days and is known as the evection.

### Maps in the Circular Restricted Three-Body Problem

One now adopts a normalized system of units based on the Earth-Moon system: unit mass = (Earth + Moon), lunar mass = $\mu = 0.0215$, unit distance = 384,410 km, unit time = 104.362 h, unit velocity = 1023.17 m/s, unit acceleration = 0.00273 m/s$^2$. The lunar radius $r_m = 0.00452133$.

One initially considers achromatic trajectories in the planar circular restricted three-body problem, the equations being given in Moon-centered coordinates:

$$\ddot{x}-2\dot{y}=\Omega_x \qquad \ddot{y}+2\dot{x}=\Omega_y \quad (6a)$$

$$\Omega = \tfrac{1}{2}[(x+1-\mu)^2+y^2] + (1-\mu)/r_1 + \mu/r_2 \quad (6b)$$

$$r_1{}^2 = (x+1)^2+y^2 \qquad r_2{}^2 = x^2+y^2 \quad (6c)$$

The achromatic trajectory of Fig. 3 has its focus point L2 located at ($x=0.167833$, $y=0$) and originates with a due-east launch from $\lambda = 0.577768148$ with $V_T = 2.28268684$. Because the trajectory is achromatic, the last value is not critical. Hence as an initial test, Eqs. (6) were integrated with the cited $\lambda$ and with $V_T = 2.285$.

The integrations of this paper were performed on a CDC 3300 computer, in the 36-bit-word mode, corresponding to 10 to 11 significant figures of accuracy. The integration step was 0.0001 for $r_2 < 3r_m$, 0.003 for greater $r_2$. Parallel integrations were performed upon two trajectories, with respective velocities $V_T$, $V_T + 0.001$; the focus point was found via Eqs. (3). For the initial test integration, the focus point was determined as ($x=0.16778$, $y=0.00002$), which accuracy was regarded as acceptable.

Because Eqs. (6) are planar, the cylindrical representation of Fig. 5 reduces to a two-sided plane which is referred to as the "flat cylinder;" this terminology is used because maps of certain parameters, which will be exhibited, resemble perspective drawings of three-dimensional cylinders and must be distinguished from them. Figure 6 is a map on the flat cylinder of focus points associated with several values of $V_T$ and of

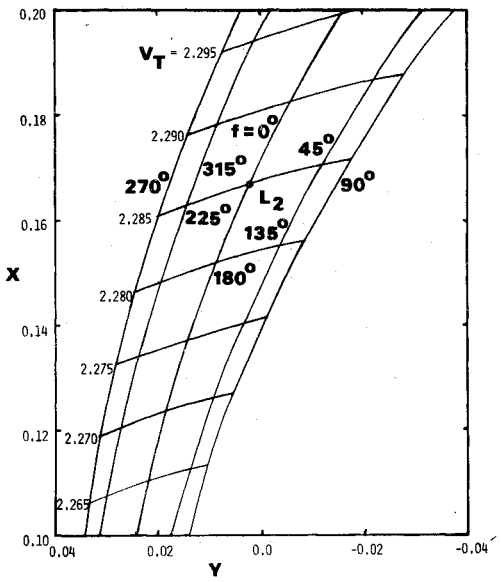


Fig. 6 Map on the flat cylinder of focus loci in the restricted three-body problem; $\Delta\lambda$ corresponds to $e_m = 0.0549$.

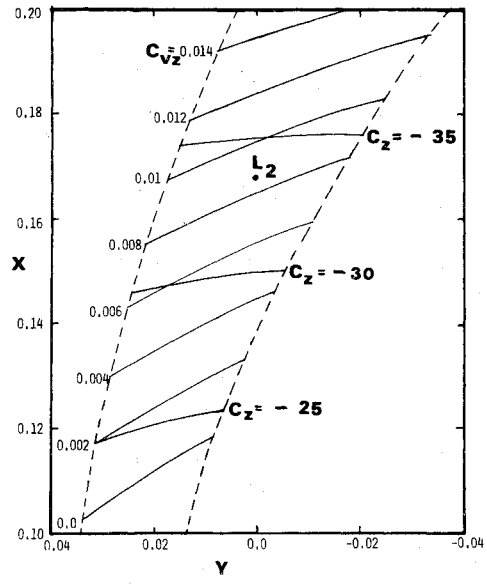


Fig. 8 Map on the flat cylinder of $C_Z$ and $C_{VZ}$ in the restricted three-body problem.

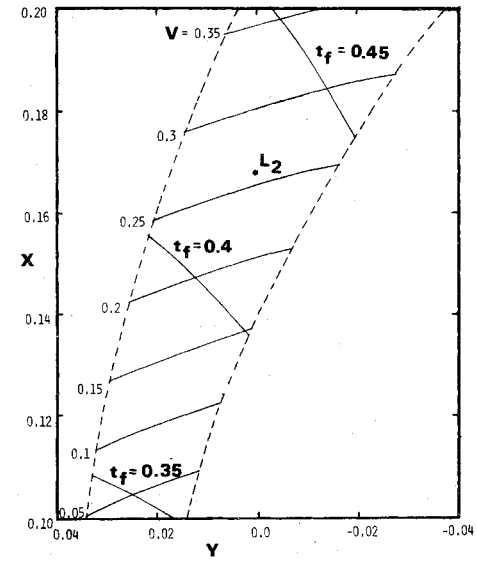


Fig. 7 Map on the flat cylinder of flight time $t_f$ and arrival velocity $V$ in the restricted three-body problem.

lunar true anomaly $(f_m)_0$ at launch, with $(f_m)_0$ and $\Delta\lambda$ being related by Eqs. (5). Hence, curves of constant $(f_m)_0$ (denoted $f$) are equivalent to curves of constant $\lambda$.

Focus loci of constant $\Delta\lambda$ do not correspond to traces of trajectories; each point on such a locus corresponds to a different $V_T$ and, hence, has a distinct value of Jacobi constant. But from Fig. 4, each point on such a locus is tangent to a trajectory and, hence, indicates the direction of the mass-stream from the Moon.

It was noted earlier that there exist points for which the two trajectories are locally tangent while crossing. The locus of these points is found to coincide closely with the curve $V_T = 2.275$. At such points, miss distance $\Delta y$ is cubic in $\epsilon$ rather than being quadratic as in Eq. (4). At isolated points, one may have $\Delta y \propto \epsilon^4$; but points with $\Delta y \propto \epsilon^5$ cannot exist.

A variety of other variables were computed along the trajectories and mapped. Figure 7 gives contours of flight time and arrival velocity at the target point, mapped in coordinates $x$, $y$ on the flat cylinder (dotted outline). This map emphasizes the distinction between trajectories and constant-$\Delta\lambda$ focus loci, because velocity $V$ increases markedly with increasing $x$. Along a trajectory, by contrast, $V$ decreases slightly with increasing $x$. The low-velocity focus points involve trajectories which curve back toward the Moon, rather than escaping.

To consider the effects of variation in launch site latitude, Fig. 8 gives information on the miss sensitivity due to errors in launch $z$ and $V_Z$. The associated coefficients are denoted (see Ref. 1) $C_Z$ and $C_{VZ}$. The variations in $C_Z$ reflect the radial geometry of the problem, being close to the value $r_2/r_m$. Their negative values reflect the fact that trajectories launched initially tangent to the equator, with $\beta > 0$, cross the equator at their descending nodes and subsequently possess ground tracks over lunar southern latitudes. Such an effect does not occur for $C_{VZ}$, for which the gradient is larger in magnitude. The curve $C_{VZ} = 0.0$ corresponds to trajectories which are achromatic with respect to errors both in $V_T$ and $V_Z$.

The data of Fig. 8 were obtained by integrating Eqs. (6) together with linearized out-of-plane variational equations:

$$\ddot{z}_{a,b} + z_{a,b}\left(\frac{1-\mu}{r_1^3} + \frac{\mu}{r_2^3}\right) = 0 \qquad (7)$$

subject to initial conditions

$$z_a(0) = 1 \qquad \dot{z}_a(0) = 0 \qquad z_b(0) = 0 \qquad \dot{z}_b(0) = 1 \qquad (8)$$

and $C_Z$, $C_{VZ}$ are, respectively, the values of $z_a$, $z_b$ at a focus point. Equation (7) would be the true out-of-plane equation of motion if, in Eqs. (6), one had $r_1^2 = (x+1)^2 + y^2 + z^2$, $r_2^2 = x^2 + y^2 + z^2$. Neglecting the $z^2$ terms makes Eq. (7) linear in $z$ so it is a variational equation and not an equation of motion.

### Maps in the Elliptic Restricted Three-Body Problem

The shift in $\lambda$, associated with lunar libration in latitude, is a result of lunar eccentricity; hence it cannot be completely accounted for outside of a dynamical model which takes $e_m$ explicitly into account. Such a model is the elliptic restricted three-body problem; this model then takes account of virtually all perturbations on the trajectories, for as shown in Ref. 1, residual perturbations (solar effects) are quite small.

There is ordinarily no advantage in using the elliptic rather than the circular restricted problem, in preliminary investigations such as the present study. The equations are more complex, and the Jacobi integral does not exist as an algebraic function of the state-vector components. This is because of

the explicit presence of the independent variable $f_m$, lunar true anomaly, in the equations. Moreover, the presence of $f_m$ adds an additional degree of freedom to the system, insofar as an initial value must be specified. But, for the present problem, it is possible to define a renormalization of the initial conditions at launch, such that these condition are expressed uniquely and in a convenient manner, as functions of $f_m$ which are physically related to the initial choice $f_m = 0$.

In this model the in-plane coordinates $x, y$ "pulsate," being normalized with respect to the variable Earth-Moon distance, and rotate at rate $df_m/dl_m$, $l_m$ being the lunar mean anomaly:

$$x = W\bar{x} \qquad y = W\bar{y} \qquad df_m/dl_m = W^2(1-e_m{}^2)^{1/2} \tag{9}$$

where

$$W = (1+e_m\cos f_m)/(1-e_m{}^2)$$

$\bar{x}, \bar{y}$ are nonpulsating rotating coordinates. There is the mean value, $e_m = 0.0549$. Then, with $(\,)' = d(\,)/df_m$,

$$x'' - 2y' = \Omega_x \qquad y'' + 2x' = \Omega_y \tag{10a}$$

$$\Omega = (1+e_m\cos f_m)^{-1}\{\tfrac{1}{2}[(x+1-\mu)^2 + y^2] + (1-\mu)/\rho_1 + \mu/\rho_2 \tag{10b}$$

$$\rho_1{}^2 = (x+1)^2 + y^2 \qquad \rho_2{}^2 = x^2 + y^2 \tag{10c}$$

and again L2 exists at ($x = 0.167833$, $y = 0$). Equations (10) were integrated subject to the initial conditions

$$(f_m)_0 = n\pi/4 \qquad (n = 0,1,2,\ldots,8) \tag{11a}$$

$$\lambda_0 = 0.577768148 + \Delta\lambda[(f_m)_0] \qquad \Delta\lambda = \text{Eq. (5)} \tag{11b}$$

$$r_m = 0.00452133 W_0 \qquad W_0 = W[(f_m)_0] \tag{11c}$$

$$x_0 = -r_m\cos\lambda_0 \qquad y_0 = -r_m\sin\lambda_0 \tag{11d}$$

$$V_0 = 2.265 + 0.005m \qquad (m = 0,1,2,\ldots,8) \tag{11e}$$

$$x'_0 = [(V_0\sin\lambda_0)W_0 + x_0 W'_0]/W_0{}^k \tag{11f}$$

$$y'_0 = [(-V_0\cos\lambda_0)W_0 + y_0 W'_0]/W_0{}^k \tag{11g}$$

$$W'_0 = -[e_m\sin(f_m)_0]/(1-e_m{}^2) \tag{11h}$$

and $k$ is chosen such that maps of parameters, akin to Figs. 6-8, may be generated for the selected values of $(f_m)_0$, $V_0$ so as to avoid giving a large variation due to $e_m \neq 0$. The value $k = 2.0$ was found by numerical experiment to give good results. Equations (11) then define the renormalized initial conditions, which permit study of Eqs. (10) with virtually the same convenience as Eqs. (6). The renormalization involves the initial conditions only and not the equations of motion; it is possible to select dependent and independent variables which reduce Eqs. (10) to a simpler form than is provided by the standard choice, Eqs. (9).[7] Moreover, Eqs. (9) lead to the standard normalization of velocities which is $x', y'$ in Eqs. (11) with $k = 0$. Since this standard normalization applies to velocities subsequent to launch, numerical designation of normalized velocities will involve the suffix $R$. Thus, "$V_T = 2.285R$" refers to an initial condition for which $V_0 = 2.285$; "$V = 0.259$" refers to a subsequent condition for which $(x'^2 + y'^2)^{1/2} = 0.259$.

Figure 9 is the counterpart of Fig. 6, being a mapping onto the flat cylinder of focus loci for achromatic trajectories with cited values of $V_0$ and $(f_m)_0$. There is evident similarity to Fig. 6. The map is divided to right and left of L2, which confirms the suitability of $\lambda_0$ for the launch site. There is

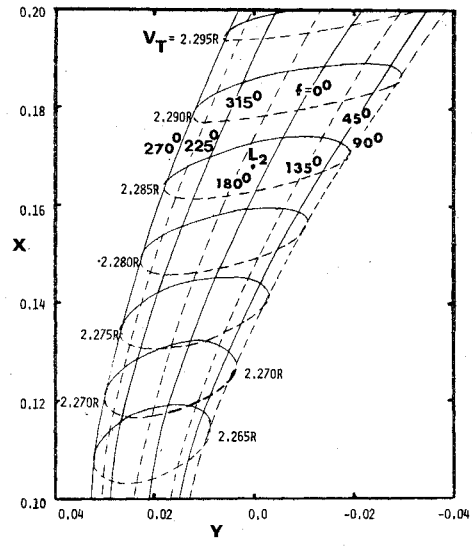


**Fig. 9 Same as Fig. 6 except in the elliptic restricted problem.**

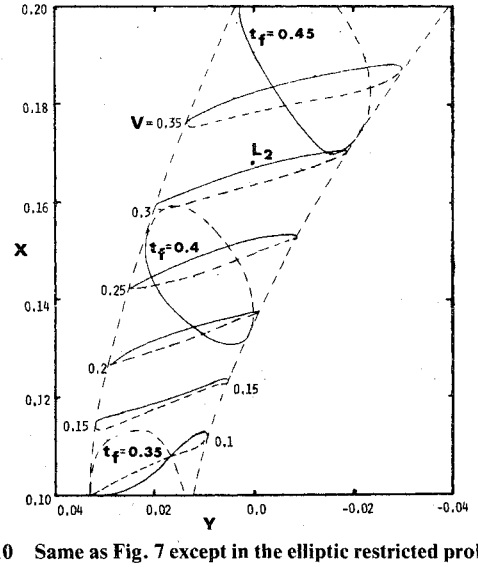


**Fig. 10 Same as Fig. 7 except in the elliptic restricted problem.**

slight unevenness; the loci with $(f_m)_0 = 0$ deg, 180 deg pass, respectively, right and left of L2 with miss distances of $-0.00291$, $0.00250$. So a more accurately centered map results by displacing the launch site eastward by 0.001221 rad or 2.123 km. Again, there exists a locus of points where pairs of computed orbits (respectively, with renormalized launch velocities $V_0$ and $V_0 + 0.001$) are tangent while crossing, this locus lying close to the curve $V_T = 2.275R$.

Figure 10 is the counterpart of Fig. 7; the flight times $t_f$ are the elapsed increases in $f_m$ subsequent to launch. Figure 11 is the counterpart of Fig. 8 and is found in the same way, except that the counterpart of Eqs. (7) is written[8]

$$a''_{a,b} + z_{a,b}(1+e_m\cos f_m)^{-1}\left(e_m\cos f_m + \frac{1-\mu}{\rho_1{}^3} + \frac{\mu}{\rho_2{}^3}\right) = 0 \tag{12}$$

and $\rho_{1,2}$ are as in Eqs. (10) while Eqs. (12) are integrated with the initial conditions of Eq. (8). In Fig. 11 again there is a locus of points for which trajectories are achromatic with respect to both $V_T$ and $V_Z$, and which is close to the locus of this type in Fig. 8.

In Figs. 9-11, there are no fundamental differences with respect to their counterparts. The shapes of the loci reflect the additional degree of freedom associated with the choice of

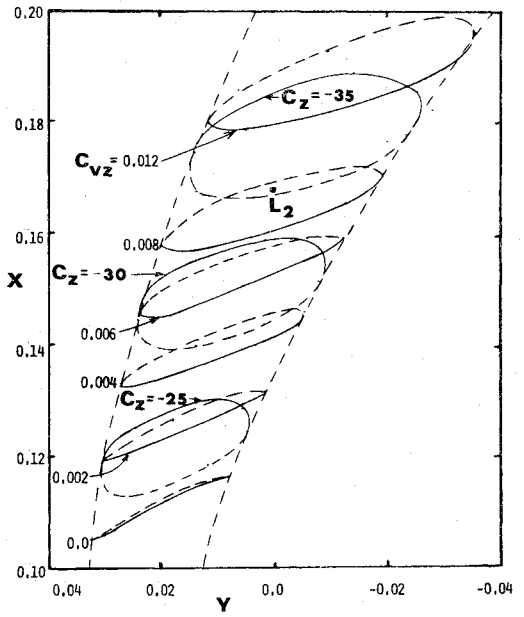


**Fig. 11 Same as Fig. 8 except in the elliptic restricted problem.**

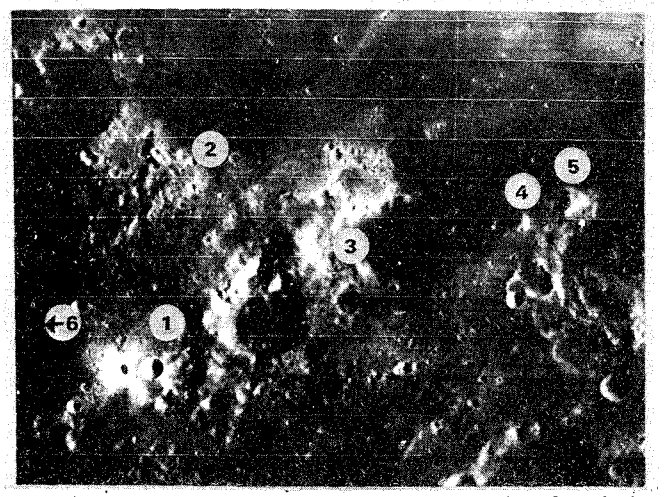


**Fig. 12 Medium-resolution photography of the optimal launch site (point 1) and its vicinity; see text for discussion of other points. The two bright craters directly south of point 1 are Censorinus and Censorinus-A; the large crater due east of point 1 is Maskelyne-A. Mare Tranquillitatis is to the north. North is to the top; scale, 1: 1,800,000 (1 mm = 1.8 km).**

$(f_m)_0$. One cannot take out all the associated variation without a more complex renormalization than Eqs. (11), but one can reduce the variation so as to prevent it from being a serious inconvenience.

## System Applications

In considering engineering aspects of lunar mass transport, the mass-catcher has not been well defined, but some attention has been given to the self-propelled bag approach. Representative features of this concept include[3]: target diameter = 100 m, total capacity = 100,000 tons (1 ton = $10^3$ kg), empty mass ~1500 tons, fill time = 1 month, onboard power = 25 MW, and onboard thrust ~12,000 N ($I_{sp}$ = 405 s). The key considerations here are its widely variable mass, its target diameter, its maneuver capability, and its capability for catching high-velocity payloads. Thus, consider application of the results of the trajectory computations to the definition of operational considerations for this catcher and for the mass-driver.

### Mass-Driver Accuracy

The preceding computations permit assessment of required mass-driver accuracy. In Fig. 3 one has: $\Delta x = V\Delta t_2$, where $\Delta t_2$ is as in Eq. (3), if $\Delta t_1 = 0$. (In general, $\Delta x = V(\Delta t_2 - \Delta t_1)$, where $\Delta t_2 - \Delta t_1$ is a slowly varying quantity proportional to $\epsilon$). Also, again from Fig. 3 and Eq. (3): $\Delta\gamma = (\dot{x}_2\dot{y}_1 - \dot{x}_1\dot{y}_2)/V^2$. Hence there is the result

$$\Delta y/\epsilon^2 = C_{VT2} = \frac{\dot{x}_2\dot{y}_1 - \dot{x}_1\dot{y}_2}{\epsilon^2 V}(\Delta t_2 - \Delta t_1)\cdot 0.03671919 \quad \text{m/(cm/s)}^2 \qquad (13)$$

The normalizing factor of 0.036719 converts Eq. (13) from dimensionless units to metric units; numerically, $C_{VT2}$ then is the miss $\Delta y$ in meters, due to an $\epsilon$ of 1 cm/s. At L2, $C_{VT2} = 0.1956$ m/(cm/s)$^2$; in the region of interest, roughly $0.12 \le x \le 0.2$, $C_{VT2} < 0.3$. (Near $V_T = 2.275$, $C_{VT2} = 0$ as noted earlier.) Thus an $\epsilon$ of 10 cm/s gives $\Delta y < 30$ meters during mission operations. This is four orders of magnitude better than is achieved using nonachromatic trajectories.[1]

Equation (13) holds for planar motion and requires modification for the effects of initial inclination of the motion at launch, with respect to the lunar equator, produced (for example) by lunar obliquity. Thus, if $\psi$ is the inclination angle in radians, taking $C_{VZ} = 0.01$ as reference value, and with reference miss distance $\Delta z = 40$,

$$\epsilon = 0.10\left(\frac{0.01}{C_{VZ}}\right)\left(\frac{\tan 0.1}{\tan\psi}\right)\left(\frac{\Delta z}{40}\right) \text{ m/s} \qquad (14)$$

and Eq. (14) reflects the scatter in arrival $z$ due to $\Delta V_Z = \Delta V_T \tan\psi$; an additional component of scatter results from uncorrelated (intrinsic) variations in $\Delta V_Z$ at launch. For a due-east launch, with $\psi \le 6.9$ deg due to lunar obliquity, Eq. (13) may provide the limit on $\epsilon$. It must also be noted that variations in $\Delta V_N$ must be held an order of magnitude lower than variations in $\Delta V_Z$, owing to the correspondingly greater $C_{VN}$ found in Ref. 1. Reference 2 proposed the intrinsic limits on allowed $\Delta V_N$, $\Delta V_Z$ as, respectively, 0.1, 1.0 cm/s. From an engineering standpoint the correction and control of $\Delta V_N$, $\Delta V_Z$ are identical problems insofar as both errors are normal to the mass-driver track and to the initial flight path. Consequently, success in controlling $\Delta V_N$ will permit control of the intrinsic $\Delta V_Z$ such that virtually all $\Delta V_Z$ will arise as $\Delta V_Z = \Delta V_T \tan\psi$.

### Mass-Driver Siting and Aim Direction

From Fig. 9, the optimal site is equatorial and at longitude 33 deg, 10.42 min E. Such a site is associated with focus-locus maps, on the flat or three-dimensional cylinder, which are accurately centered at L2 for mean $e_m$. Since the catcher motion is heavily constrained by such maps, any offset in them, from being centered at L2, results in increased catcher accelerations being required to maintain the offset, as is discussed elsewhere.[3] In particular, for an out-of-plane offset $\Delta x$, $\Delta\ddot{z} = -3.19042\,\Delta z$.[8]

For use in site assessment and evaluation, there exists a considerable body of high-quality spacecraft photography of the cited location and of its environs, including: Lunar Orbiter – I-41M, I-42M, I-48M, I-49M, IV-73H$_1$, V-55M to V-63M, V-55H to V-63H; and Apollo mapping camera – AS15-2546 to -2548 and AS15-2680 to -2687. Figure 12 (LO IV-73H$_1$) shows the site, point 1, as lying near the north rim of the crater Censorinus, in rugged country. This site has several unfavorable features. It lies atop a ridge almost due north of Censorinus and just west of the high crater wall of Maskelyne-A. So it is not possible to launch tangentially without striking this wall. Moreover, an oblique launch appears difficult to achieve since the mass-driver cannot readily be angled upward. Figure 12 further shows that the rugged, unfavorable terrain and the Maskelyne crater wall extend north for at least

a degree of latitude, while to the south the terrain is even more rugged and crater-pocked.

Figure 12 suggests that much more favorable conditions exist in the V-shaped bay of Mare Tranquillitatis lying due north of Maskelyne-A. Detailed site photography (LO I-48M) confirms that this location, point 2, represents typical mare terrain and thus is quite satisfactory in its topography. It also lies at a boundary between geochemically different highland and mare regions, permitting access to diverse mineral types. The coordinates are $\lambda = 33$ deg, 40 min E by $\beta = 1$ deg, 44 min N. At L2 the offsets are $\Delta y = 0.00146$, $\Delta z = -0.00457$.

This offset in $\Delta z$ is reduced by angling the launch direction northward from due east by an angle $\psi$. The catcher then requires the following thrust for stationkeeping:

$$m(t)\Delta\ddot{z} = [0.0412(V_T \tan\psi \, dC_{VZ}/dx + r_m \sin\beta \, dC_Z/dx)]$$

$$-m(t)[3.19042(V_T C_{VZ}\tan\psi + r_m C_Z \sin\beta)] \qquad (15)$$

where the bracketed terms are denoted $A$, $B$, respectively. In $B$, the terms in parentheses give the offset in $z$. In $A$, the terms in parentheses give the rate of upward rise $dz/dx$ of the mass-stream. The coefficient $0.0412 = 0.259/2\pi$ is the normalized acceleration due to the momentum flux of a mass-stream with $V = 0.259$ at L2 on a catcher which loads in one month. Also, $m(t)$ is the fractional catcher mass (when full, $m = 1$) and it is convenient to take $m = t/2\pi$, i.e. the catcher loads uniformly during the month. At L2, from Figs. 6-9, $V_T = 2.285$, $C_{VZ} = 0.00851$, $C_Z = -33.46$, $dC_{VZ}/dx = 0.2$, $dC_Z/dx = -1/r_m$.

If $\Delta V$ is the velocity change required by a *loaded* catcher to maintain the $\Delta z$ offset,

$$\Delta V = \int_0^{2\pi} \Delta\ddot{z} m(t)\, dt$$

Then

$$\Delta V = 2\pi(A - \tfrac{1}{2}B) \qquad (A \geq B) \qquad (16a)$$

$$\Delta V = 2\pi(A^2/B - A + \tfrac{1}{2}B) \qquad (A < B) \qquad (16b)$$

So for $\psi = 0$ deg, $\Delta V = 0.03805$. By optimization, the minimum $\Delta V = 0.01365$ for $\psi = 18.306$ deg. On the other hand, this value, together with effects of lunar obliquity, gives a maximum launch inclination of 24.985 deg, for which $\Delta V_Z = 0.466\ \Delta V_T$. Consequently there exists a tradeoff between required accuracy on $V_T$ and reduction of $\Delta V$ at the catcher.

Similar considerations apply to point 3: $\lambda = 35$ deg E by $\beta = 0$ deg, 48 min N. Point 3 is of interest because trajectories could pass either or both of the mountains 4 and 5. On such mountains, downrange-corrector stations could detect launch errors and correct them.[3] Point 6 is actually a range of equatorial sites extending eastward into the Sea of Tranquillity, from which trajectories could pass over the mountain adjacent to point 1. Specific selection of a longitude near points 3 or 6 then would rely upon details of the topography of these downrange mountains.

**Catcher Equations**

Now consider the three-dimensional motion of the catcher as structured by Figs. 6-8. These data will be used to derive a linear equation for catcher motion, valid near L2.

The catcher is considered to fill uniformly. Its mass-change rate is $\dot{m} = m_f/2\pi$ ($m_f$ = final mass) and at any time, $m = \dot{m}t$; due to this mass-flux the catcher then suffers acceleration components

$$a_x = (1/t)(V\cos\theta - \dot{x}) \qquad (17a)$$

$$a_y = (1/t)(V\sin\theta - \dot{y}) \qquad (17b)$$

$$a_z = (1/t)(V\, dz/dx - \dot{z}) \qquad (17c)$$

where $\theta$ = angle of the mass-flux direction measured counterclockwise from the positive $x$ axis. Here $\theta = -25.4588$ deg $+ \Delta\lambda + \Delta\lambda_0$; $-25.4588$ deg $\equiv \theta_0$ is the computed $\theta$ for $f = 0$ in Fig. 6; $\Delta\lambda$ is Eq. (5); $\Delta\lambda_0$ is the offset in launch site longitude from the nominal $\lambda_0$ (point 1 in Fig. 12). Also $\dot{x}$, $\dot{y}$, $\dot{z}$ are components of catcher velocity. Effects of the potential field are given by linearizing Eqs. (6) about L2. Together with Eqs. (17), and with L2 as the origin,

$$\ddot{x} - 2\dot{y} - 7.38084x - a_x = F(t) \qquad (18a)$$

$$\ddot{y} + 2\dot{x} + 2.19042y - a_y = G(t) \qquad (18b)$$

$$\ddot{z} + 3.19042z - a_z = H(t) \qquad (18c)$$

and $F(t)$, $G(t)$, $H(t)$ are control accelerations required to cause the catcher to follow a nominal path.

To express $V$ as a function of $x$, $y$, one has recourse to graphical measurements from Fig. 7, giving

$$V = 0.259 + 3.13x + 0.89y \qquad (19)$$

It now is necessary to constrain the motion by requiring $y = y(t)$, $z = z(t)$ to be such that at any time, the catcher is to lie upon a focus locus, on the cylinder of Fig. 5, which is a contour of constant $\Delta\lambda$ or $(f_m)_0$; then, the catcher can always be reached via an achromatic trajectory from the mass-driver. Then for $y(t)$,

$$y - x\sin\theta_0 - (x_{L2} + x)\Delta\lambda_0 = y_{\max.}\cos(t + \delta_0 + \Delta t_f) \qquad (20)$$

where $x_{L2} = 0.167833$; $\delta_0$ is a fixed phase angle which may be optimized from operational considerations; $\Delta t_f$ is the time delay associated with variations in the payloads' flight times. By graphical construction from Figs. 6 and 7, there is approximately

$$y_{\max.} = 2e_m(x_{L2} + x) \qquad \Delta t_f = x - y \qquad (21)$$

Then $y = y(x; t)$ and, retaining linear terms,

$$y = \frac{x\sin\theta_0 + (x_{L2} + x)[2e_m(\cos\tau - x\sin\tau) + \Delta\lambda_0]}{1 - 2e_m(x_{L2} + x)\sin\tau}$$

$$= K(t)x + D(t) \qquad (22)$$

where $\tau = t + \delta_0$.

Now consider the out-of-plane motion with the following angles: $\beta$ = launch site latitude, $\phi$ = libration phase angle, $\psi$ = launch inclination angle [Eq. (15)], $\gamma$ = lunar obliquity = 6 deg, 40 min, 44s.

$\phi$ results from the slightly different libration periods associated with the librations in longitude and latitude, respectively; $\phi$ circulates through 360 deg with a period of 5.97037 years. Then,

$$z = r_m C_Z \sin(\beta + \gamma\sin T) + V_T C_{VZ}\tan(\psi + \gamma\cos T) \qquad (23)$$

where $T = t + \delta_0 + \phi$. From graphical measurements on Figs. 6-8,

$$V_T = 2.285 + 0.375x + 0.095y \qquad (24a)$$

$$C_{VZ} = 0.00851 + 0.0200x + 0.078y \qquad (24b)$$

and it is convenient to take $V_T = 2.285$ (constant), $C_Z = -(x + x_{L2})/r_m$, and to use the small-angle approximations on $\beta$, $\psi$, $\gamma$. One then has

$$z = P(t)x + Q(t) \qquad (25)$$

which is the counterpart of Eq. (22).

In Eqs. (18), one can then eliminate $a_x$, $a_y$, $a_z$; $y$, $\dot{y}$, $\ddot{y}$; $z$, $\dot{z}$, $\ddot{z}$ in favor of terms in $x$, $\dot{x}$, $\ddot{x}$, $t$ and thereby obtain the linearized catcher equations. From the given developments, these equations take the form

$$\ddot{x}+f_1(t)\dot{x}+f_2(t)x+f_3(t)=F(t) \tag{26a}$$

$$g_0(t)\ddot{x}+g_1(t)\dot{x}+g_2(t)x+g_3(t)=G(t) \tag{26b}$$

$$h_0(t)\ddot{x}+h_1(t)\dot{x}+h_2(t)x+h_3(t)=H(t) \tag{26c}$$

where

$$f_1(t)=1/t-2K$$

$$f_2(t)=-2\dot{K}-7.38084 - (1/t)(3.13+0.89K)\cos(\theta_0+\Delta\lambda+\Delta\lambda_0)$$

$$f_3(t)=-2\dot{D}-(1/t)(0.259+0.89D)\cos(\theta_0+\Delta\lambda+\Delta\lambda_0)$$

$$g_0(t)=K$$

$$g_1(t)=2\dot{K}+2+K/t$$

$$g_2(t)=\ddot{K}+2.19042K + (1/t)[\dot{K}-(3.13+0.89K)\sin(\theta_0+\Delta\lambda+\Delta\lambda_0)]$$

$$g_3(t)=\ddot{D}+2.19042D + (1/t)[\dot{D}-(0.259+0.89D)\sin(\theta_0+\Delta\lambda+\Delta\lambda_0)]$$

$$h_0(t)=P$$

$$h_1(t)=2\dot{P}+P/t$$

$$h_2(t)=\ddot{P}+3.19042P+(1/t)[\dot{P}-P(3.13+0.89K)]$$

$$h_3(t)=\ddot{Q}+3.19042Q+(1/t)[\dot{Q}-P(0.259+0.89D)]$$

and where

$$K=(1+2e_m x_{L2}\sin\tau)\sin\theta_0+2e_m(\cos\tau-x_{L2}\sin\tau) + 4e_m{}^2 x_{L2}\sin 2\tau-x_{L2}\sin^2\tau)+(1+4e_m x_{L2}\sin\tau)\Delta\lambda_0$$

$$D=2e_m x_{L2}(\cos\tau+e_m x_{L2}\sin 2\tau)+(1+4e_m x_{L2}\sin\tau)x_{L2}\Delta\lambda_0$$

$$P=-(\beta+\gamma\sin T)+2.285(0.2+0.078K)(\psi+\gamma\cos T)$$

$$Q=-x_{L2}(\beta+\gamma\sin T) + 2.285(0.00851+0.078D)(\psi+\gamma\cos T)$$

Among the applications of Eqs. (26) are the following:

1) They serve to determine the control acceleration components $F(t)$, $G(t)$, $H(t)$ for operational control programs $x=x(t)$, thus permitting design of the thrustor systems and determination of associated power requirements.

2) By defining $\ddot{x}$ as a control variable, it is possible to develop optimal catcher trajectories near L2, in the sense that an appropriate cost function, involving $F(t)$, $G(t)$, $H(t)$, is minimized.

3) From Fig. 7 it is seen that for $x$ near 0.11, catching can be done with low payload impact velocity. Moreover, if may be proposed to gain operational advantage from use of a mass-driver site other than point 1 of Fig. 12. Equations (26) then permit assessment of the design tradeoffs involved in such concepts.

4) From Fig. 6 or Eq. (24), a solution to Eqs. (26) can be interpreted in terms of an operational launch program $V_T=V_T(t)$ required at the mass-driver.

5) By assuming a more general mass-fill-rate law, one may consider the possible advantages of using a variable mass-flux as a control upon the motion of the catcher.

Consequently, further results in preliminary studies of lunar mass transport will rely principally upon consideration of Eqs. (26). Such results are reported elsewhere.[3]

## Conclusions

The concept of achromatic trajectories is seen to provide a point of departure whereby one may undertake a description of the operational problems associated with the trajectory dynamics of one means of lunar mass-transport. In particular, this concept leads to the derivation of the catcher equations, which contain information needed for studies of the operational motion of the mass-catcher, including optimal trajectories, propulsion system requirements assessment, alternate catching strategies, and operational mass-driver launch velocity programs. There thus appear to be no obstacles to an improved conceptual understanding of the use of the mass-driver/mass-catcher system, as a means for the large-scale transport of lunar material and lunar resources.

## Acknowledgments

This work was conducted at the Max-Planck-Institut für Kernphysik, Heidelberg, West Germany. The author wishes to thank Gerd Dräger for his assistance in computation, and the people of the Max-Planck-Institut für Kernphysik for their many courtesies during the present research. This work was supported through a research fellowship with the Alexander von Humboldt Foundation, Bonn, West Germany.

## References

[1] Heppenheimer, T. A. and Kaplan, D., "Guidance and Trajectory Considerations in Lunar Mass Transportation," *AIAA Journal*, Vol. 15, April 1977, pp. 518-525.

[2] O'Leary, B. T., Heppenheimer, T. A., and Kaplan, D., "Trajectory Analyses for Material Transfer from the Moon to the Space Manufacturing Facility," *Space-Based Manufacturing from Nonterrestrial Materials*, edited by G. K. O'Neill, Progress in Aeronautics and Astronautics, Vol. 57, AIAA, New York, 1977.

[3] Heppenheimer, T. A., "A Mass-Catcher for Large-Scale Lunar Material Transport," *Journal of Spacecraft and Rockets*, to be published.

[4] Heppenheimer, T. A., "Steps Toward Space Colonization: Colony Location and Transfer Trajectories," *Journal of Spacecraft and Rockets*, to be published.

[5] Kopal, Z., *The Moon*, D. Reidel Publishing Co., Dordrecht, Holland, 1969.

[6] Brouwer, D. and Clemence, G. M., *Methods of Celestial Mechanics*, Academic Press, New York, 1961.

[7] Heppenheimer, T. A., "A Note on Independent Variables for Restricted Three-Body Problems," *Celestial Mechanics*, Vol. 4, Dec. 1971, pp. 236-328.

[8] Szebehely, V. G., *Theory of Orbits*, Academic Press, New York, 1967.